SCIENTIFIC REPORTS

OPEN

Controlling the Two-Photon-Induced Photon Cascade Emission in a Gd^{3+}/Tb^{3+}-Codoped Glass for Multicolor Display

Received: 24 November 2015
Accepted: 18 January 2016
Published: 22 February 2016

Mao-Hui Yuan[1], Hai-Hua Fan[1], Hui Li[1], Sheng Lan[1], Shao-Long Tie[2] & Zhong-Min Yang[3]

We reported the first observation of the two-photon-induced quantum cutting phenomenon in a Gd^{3+}/Tb^{3+}-codoped glass in which two photons at ~400 nm are simultaneously absorbed, leading to the cascade emission of three photons in the visible spectral region. The two-photon absorption induced by femtosecond laser pulses allows the excitation of the energy states in Gd^{3+} which are inactive for single-photon excitation and enables the observation of many new electric transitions which are invisible in the single-photon-induced luminescence. The competition between the two-photon-induced photon cascade emission and the single-photon-induced emission was manipulated to control the luminescence color of the glass. We demonstrated the change of the luminescence color from red to yellow and eventually to green by varying either the excitation wavelength or the excitation power density.

The phenomenon of photon cascade emission or the so called "quantum cutting", in which a photon of high energy is absorbed and converted to two or more photons with lower energies, has been studied intensively in the past few decades because of its potential applications in mercury-free lamps and plasma display panels[1–9]. In recent years, this phenomenon has drawn great attention in the research and development of high-efficiency solar cells because it can significantly improve the conversion efficiency of photon to electricity and reduce heat generation[10–13]. Owing to their unique energy states, rare-earth ions, especially the lanthanide ions, are considered as promising candidates not only for photon up-conversion but also for photon down-conversion[13–22]. For example, solid state full color display[23] has been demonstrated by exploiting the photon up-conversion in three lanthanide ions of Pr^{3+}, Er^{3+}, and Tm^{3+}. In addition, the lanthanide ions have exhibited fascinating luminescent properties such as intense narrow-band emission, high conversion efficiency, broad emission peaks, much different lifetimes, and good thermal stability[8,21,24–27]. Therefore, rare-earth-ion-doped materials have been widely studied and exhibited potential application in the fields of illumination, imaging, display, solar cells, and medical radiology because such materials can be fabricated at a low cost and in large quantities[23–44].

In rare-earth-ion-doped materials, Tb^{3+}-doped glasses have been the focus of many studies because of their high luminescence efficiency at around 550 nm which is convenient for direct coupling with silicon detectors[45]. More interestingly, it has been shown that the luminescence can be further enhanced by adding Gd^{3+} into Tb^{3+}-doped glasses because of the energy transfer (ET) from Gd^{3+} to Tb^{3+}, as schematically shown in Fig. 1. In fact, the ET between Gd^{3+} and Tb^{3+} has been extensively investigated in many other different host materials[46–50]. Although electrons can be generated in Gd^{3+}, the luminescence from Gd^{3+}/Tb^{3+}-codoped glasses arises mainly from the transitions from the level $^5D_4$ to the levels $^7F_{0-6}$ in Tb^{3+} which give rise to four emission bands in the visible light region[46–50]. In Fig. 1, it is noticed that the levels ^6G_J in Gd^{3+} are located well above the high-energy levels in Tb^{3+} ($^5K_7$ etc.) while the levels ^6D_J, ^6I_J, and ^6P_J in Gd^{3+} have similar energies with some energy levels in Tb^{3+}. If the population of the levels ^6G_J in Gd^{3+} is induced, one can expect the transitions of electrons to the low-energy

[1]Guangdong Provincial Key Laboratory of Nanophotonic Functional Materials and Devices, School of Information and Optoelectronic Science and Engineering, South China Normal University, Guangzhou 510006, China. [2]School of Chemistry and Environment, South China Normal University, Guangzhou 510006, China. [3]MOE Key Laboratory of Specially Functional Materials, Institute of Optical Communication Materials, South China University of Technology, Guangzhou 510640, China. Correspondence and requests for materials should be addressed to S.L. (email: slan@scnu.edu.cn) or S.-L.T. (email: tiesl@scnu.edu.cn)

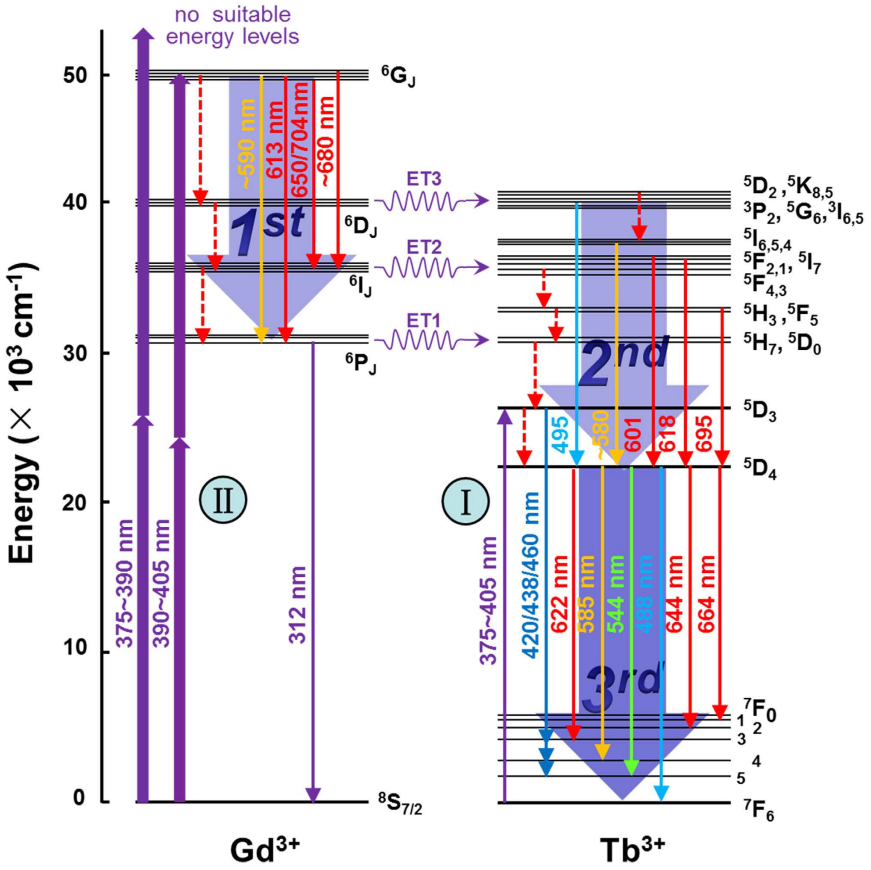

Figure 1. Energy level diagram of Gd^{3+} and Tb^{3+} in which the two-photon-induced absorption, the photon cascade emission Ⅱ, and the single photon absorption assisted by Rabi oscillation or phonons Ⅰ, and the possible electronic transitions between the energy levels are illustrated.

levels (^6D_J, ^6I_J, and ^6P_J) of Gd^{3+}, the ET of electrons from Gd^{3+} to Tb^{3+}, the transitions of electrons to the level $^5D_4$ and finally to the levels $^7F_{0-6}$. Such a cascade transition process may result in the cascade emission of photons with different energies. In practice, the population of the levels ^6G_J in Gd^{3+} can be realized by using femtosecond (fs) laser light at ~400 nm through two-photon-induced absorption (TPA). The high peak power and wide linewidth of fs laser light are highly suitable for effectively exciting the levels ^6G_J in Gd^{3+}. Actually, fs laser light at 800 nm has been used to excite the three-photon-induced luminescence in rare-earth-ion-doped glasses[37]. When fs laser light at 400 nm is used to excite the levels ^6G_J in Gd^{3+}, the level $^5D_3$ in Tb^{3+} with a wavenumber of ~26336 cm^{-1} (corresponding to a wavelength of ~381 nm) can also be populated through Rabi oscillation or phonon-assisted transition[51], leading to the conventional emission from Tb^{3+}. For excitation wavelengths (λ_{ex}) shorter than 400 nm, the population probability for the levels ^6G_J is reduced while that for the level $^5D_3$ is increased. It implies the existence of a competition between the cascade emission and conventional emission that depends strongly on λ_{ex}. On the other hand, the population of the level $^5D_3$, which is caused mainly by Rabi oscillation[51], will exhibit a strong dependence on the excitation power density (P_{ex}). Therefore, it is expected that one can manipulate the competition between the cascade emission and conventional emission and thus control the luminescence color by varying λ_{ex} or P_{ex}, exploring its applications in color display[52].

Results and Discussion

The proposed scheme was examined by using different glasses codoped with Gd^{3+} and Tb^{3+} and the dependence of luminescence color on λ_{ex} and P_{ex} was found to be a popular phenomenon (details in Supplementary Information, see Fig. S1). However, this behavior also exhibits a dependence on the concentration of Gd^{3+} and glass matrix. While the concentration of Gd^{3+} determines the photon cascade emission, the glass matrix affects the phonon-assisted processes such as the nonradiative decay or the relaxation of electrons. In this work, we show a pronounced phenomenon observed in a silicate glass with a composition of $56SiO_2$-$10Al_2O_3$-$12Li_2O$-$20Gd_2O_3$-$2Tb_2O_3$ (mol%). The ET from Gd^{3+} to Tb^{3+} was also observed in this glass (details in Supplementary Information, see Section 4).

In order to see the λ_{ex}-dependent competition, we varied λ_{ex} from 375 to 405 nm and examined the luminescence of the glass. For $\lambda_{ex} \leq 390$ nm, the luminescence always appeared to be green. However, the luminescence was changed from green to yellow when λ_{ex} was slightly shifted from 390 to 392 nm. More surprisingly, the luminescence turned to be red when λ_{ex} was further shifted to 394 nm. A comparison of the emission spectra

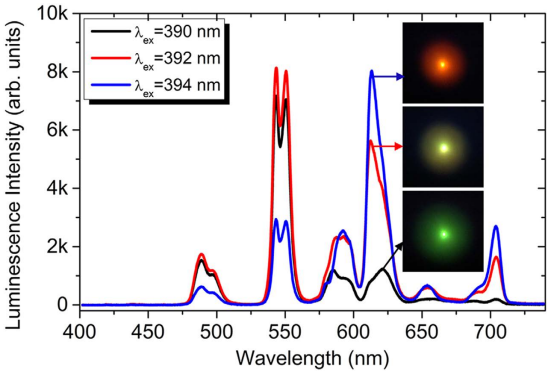

Figure 2. Comparison of the emission spectra of the glass under different λ_{ex} of 390, 392, and 394 nm. The insets show the photos of the excitation spots and the luminescence colors.

under different λ_{ex} of 390, 392 and 394 nm is presented in Fig. 2. The photos for the excitation spot are shown in the insets. It can be seen that the emission spectrum at $\lambda_{ex} = 390$ nm is dominated by the emission band at ~540 nm which corresponds to green color. For $\lambda_{ex} = 392$ nm, the relative intensities of the emission bands at ~580 nm and ~622 nm, which correspond to yellow and red colors, increase rapidly. A close inspection reveals that the peak of the emission band at ~622 nm is blue-shifted to ~613 nm. In addition, two new emission bands emerge at ~654 nm and ~704 nm, contributing to red color. For $\lambda_{ex} = 394$ nm, the intensity of the emission band at ~613 nm exceeds that of the emission band at ~550 nm and the relative intensities of the emission bands at ~654 and 704 nm are further increased, turning the color of the luminescence into red. In previous reports, the luminescence of Tb^{3+}-doped and Gd^{3+}/Tb^{3+}-codoped glasses originates mainly from the electronic transitions from the level $^5D_4$ to the levels $^7F_{0-6}$ and appears to be green. There is no report on the observation of yellow or red luminescence. Here, it is interesting that the color change in the luminescence occurs in a narrow wavelength region of 390−394 nm, which is comparable to the linewidth of the fs laser pulses (~4.0 nm).

In order to understand the underlying physical mechanism, we examined the evolution of the emission spectrum and the luminescence color with increasing P_{ex} for different λ_{ex}, as shown in Fig. 3a–c. The dependence of the luminescence intensities for different emission bands on P_{ex} was also extracted, as shown in Fig. 3d–f. For $\lambda_{ex} = 390$ nm, the luminescence color appeared to be green and remained unchanged with increasing P_{ex}. It can be seen that the intensities of the four major emission bands, which are centered at 488, 544, 585, and 622 nm, increased almost with the same rate. Consequently, the emission spectrum remained nearly unchanged except the absolute intensity. The fitting of the P_{ex} dependence of the luminescence intensity gives nearly the same slope of ~1.0 for all the emission bands, indicating that the emission is governed by single-photon process. The situation was changed for $\lambda_{ex} = 392$ nm. Two new emission bands emerged at 654 and 704 nm and the emission band peaking originally at 622 nm was blue-shifted to 613 nm. The electronic transitions related to the new emission bands (details in Supplementary Information, see Table I), which are attributed to the transitions between the high-energy levels of Gd^{3+}, were previously observed in other materials[53,54] doped with Gd^{3+} under single-photon excitation. For comparison, the glasses doped with only Gd^{3+} or Tb^{3+} were also examined under the same condition (details in Supplementary Information, see Figs S3 and S5). The slopes for the emissions bands at 488, 544, and 585 nm remained unchanged while smaller slopes were observed for the two new emission bands and the emission band at 613 nm. The change in the emission spectrum was negligible and the luminescence color remained to be yellow with increasing P_{ex}. For $\lambda_{ex} = 394$ nm, the dependence of the emission spectrum on P_{ex} became significant. It is noticed that the intensities of the emission bands at 488 and 544 nm increased in greater rates and the center of the excitation spot became yellow at high P_{ex}, as evidenced in the larger slopes of ~1.40. This behavior indicates that two-photon process has been involved in the emission process.

As mentioned above, the effective population of the levels ^6G_J can be realized by simultaneously absorbing two photons at 400 nm. For $\lambda_{ex} = 390$ nm, the population of the levels ^6G_J through TPA can be neglected because of the large energy mismatch. As λ_{ex} is red-shifted toward 400 nm, an increase in the population probability is expected. In Fig. 4, we present the evolution of the emission spectrum and the luminescence color with increasing P_{ex} measured for $\lambda_{ex} = 400$ and 405 nm. For $\lambda_{ex} = 400$ nm, the emission spectrum was similar to that observed at $\lambda_{ex} = 394$ nm. However, it is noticed that the intensity of the emission band at 613 nm became stronger than that of the emission band at 544 nm and the luminescence appeared to be red at low P_{ex}. At high P_{ex}, the intensity of the latter exceeded that of the former, changing the luminescence color to green, as shown in the inset of Fig. 4a. This behavior is also reflected in the P_{ex} dependence of the luminescence intensity shown in Fig. 4c. The slopes for the emission bands at 488 and 544 nm obtained by fitting the experimental data (1.59 and 1.64) were much larger than those for the emission bands at 590, 613, 654, and 704 nm whose slopes are reduced by nonradiative decay (details in Supplementary Information, see Fig. S6). For $\lambda_{ex} = 405$ nm, the emission spectrum was changed remarkably because of the emergence of many new emission bands, as shown in Fig. 4b. In this case, the red luminescence observed at low P_{ex} evolved gradually into green one with increasing P_{ex}, similar to that observed at $\lambda_{ex} = 400$ nm. In comparison, the slopes for the emission bands at 488 and 544 nm were reduced slightly to ~1.50 because the TPA process at $\lambda_{ex} = 405$ nm is not as efficient as that at $\lambda_{ex} = 400$ nm.

Based on the theory of colorimetry (details in the Supplementary Information, see Section 7), one can easily deduce the chromaticity coordinates for the luminescence observed under different excitation conditions and

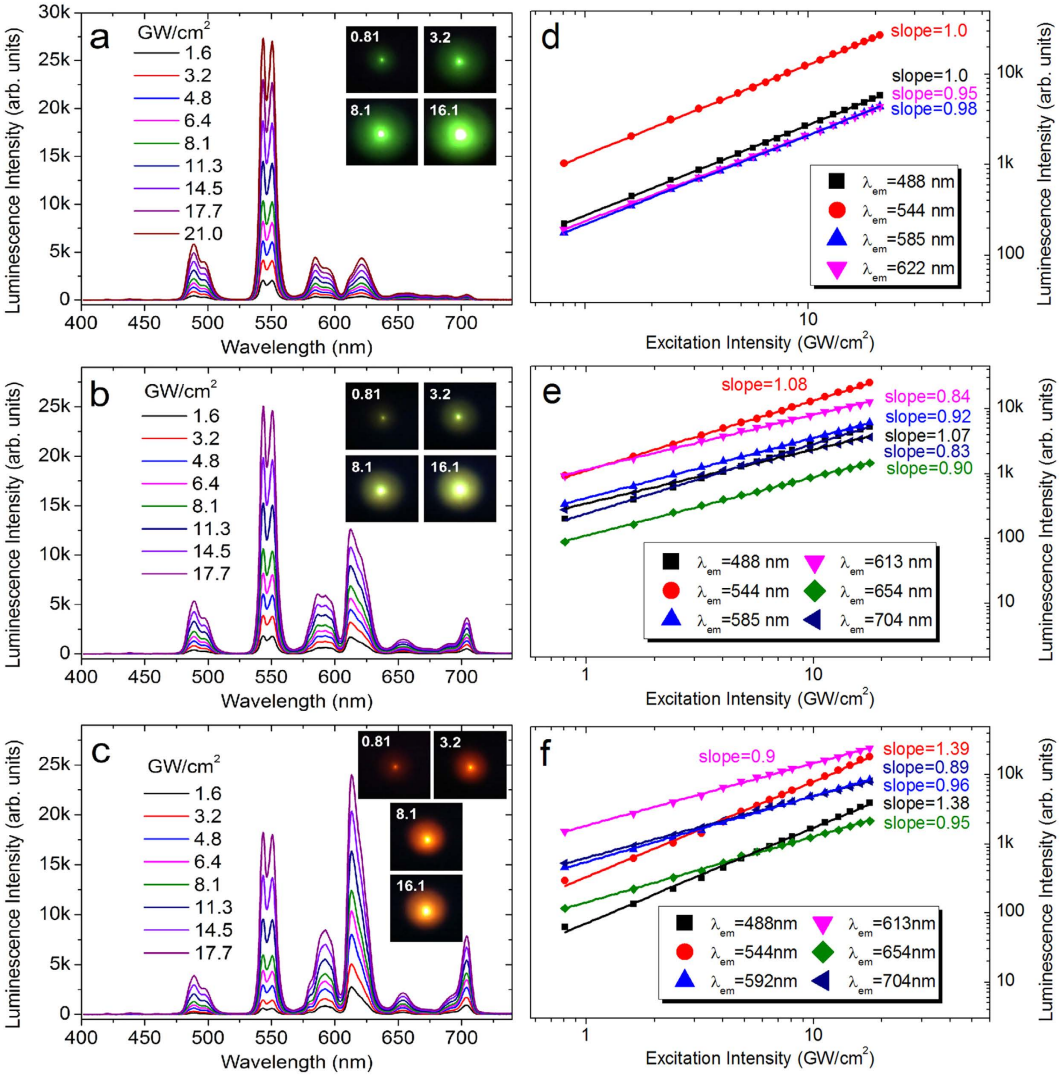

Figure 3. Evolution of the emission spectrum and the luminescence color of the glass with increasing P_{ex} under different λ_{ex} of (**a**) 390 nm, (**b**) 392 nm, and (**c**) 394 nm. The dependence of the luminescence intensities for different emission bands on P_{ex} and the fitting for the experimental data are presented in (**d**–**f**) for λ_{ex} of 390, 392, and 394 nm, respectively.

the results are shown in Fig. 5. From the Fig. 5a, under low P_{ex}, we can see that the chromaticity coordinates for $\lambda_{ex} = 390$, 392, and 394 nm appear in the green, yellow and red regions, respectively. In all cases, a shift of the chromaticity coordinate with increasing P_{ex} is found and it becomes larger for longer λ_{ex}. The largest shift of the chromaticity coordinate is observed at $\lambda_{ex} = 400$ nm, as shown in Fig. 5b. In this case, the luminescence color is changed from red to yellow and eventually to green with increasing P_{ex}.

When the levels ^6G_J in Gd^{3+} are effectively populated, the photon cascade emission is expected to dominate the emission process. It is clearly reflected in the new emission bands which correspond to the photons emitted in the cascade transition of electrons between the energy levels of Gd^{3+} and Tb^{3+}. In Fig. 6, we present a comparison of the emission spectra obtained at different λ_{ex} of 390, 392, 394, 400, and 405 nm in a logarithmic coordinate where the new emission bands originating from the photon cascade emission can be readily identified at $\lambda_{ex} = 400$ and 405 nm and indicated by arrows. In most cases, the cascade emission of three photons is observed, as shown in Fig. 1. The first photon is generated by the transition of electrons between the levels of ^6G_J and ^6I_J (or ^6P_J) in Gd^{3+}. The wavelengths of the emission photons range from 571 to 704 nm, contributing yellow or red color. The transition from the levels ^6G_J to ^6D_J in Gd^{3+} is thought to be nonradiative[53,54]. The emission of the first photon is followed by an ET process of electrons from Gd^{3+} to Tb^{3+}. Then, the emission of the second photon occurs through the transitions of electrons between the levels $^5H_3$, $^5F_{4,2,1}$, $^5I_{6,4}$, $^5K_8$ and the level $^5D_3$ or $^5D_4$. During this process, the wavelengths of the emission photons cover a broad wavelength range of 495 to 690 nm, contributing mainly yellow and red colors. The emission of the last photon occurs mainly between the levels $^5D_4$ ($^5D_3$) and $^7F_{6,5,4,3}$, contributing to green color. Although the intensities are quite weak, one can identify the new emission bands at 421, 438, and 460 which can be assigned to the transitions between the levels $^5D_3$ and $^7F_{5,4,3}$.

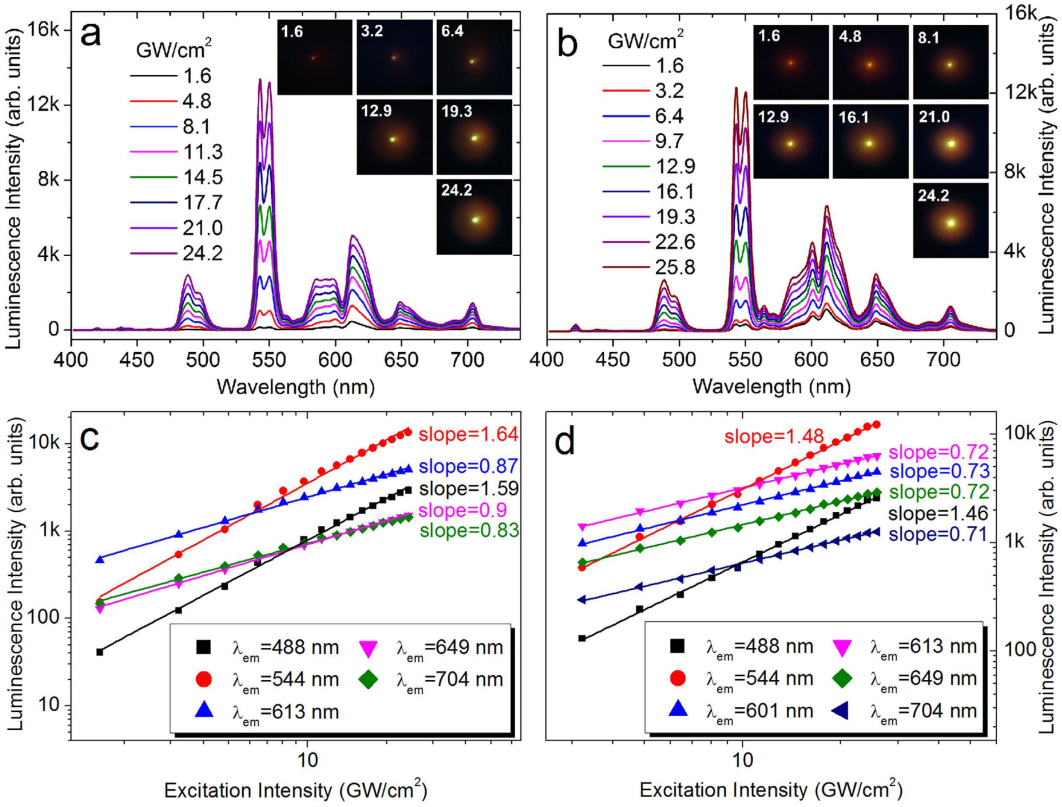

Figure 4. Evolution of the emission spectrum and the luminescence color of the glass with increasing P_{ex} under different λ_{ex} of (**a**) 400 nm and (**b**) 405 nm. The dependence of the luminescence intensities for different emission bands on P_{ex} and the fitting for the experimental data are presented in (**c**,**d**) for λ_{ex} of 400 and 405 nm, respectively.

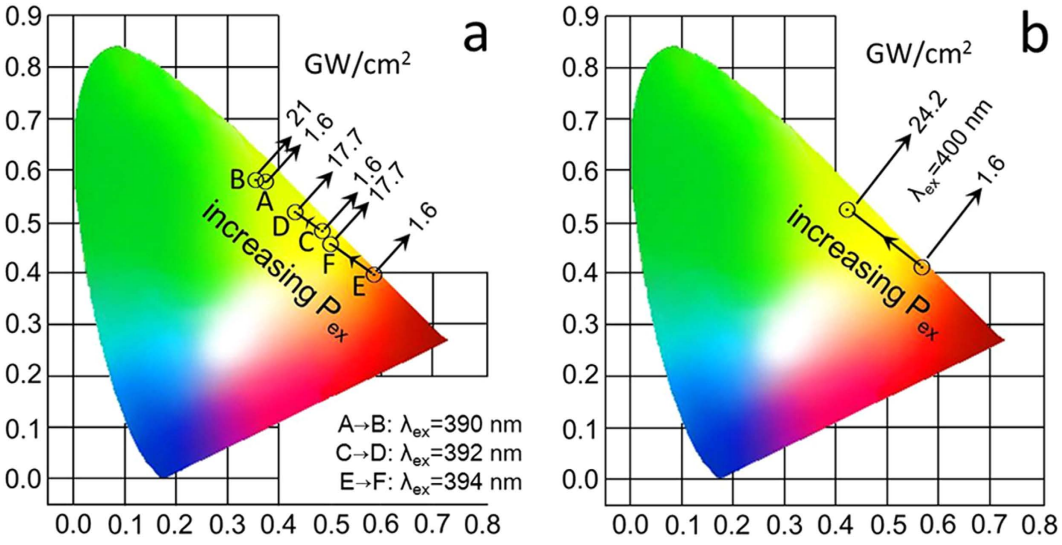

Figure 5. CIE chromaticity coordinates for the luminescence of the glass under different λ_{ex} and P_{ex}. (**a**) λ_{ex} = 390, 392, and 394 nm and (**b**) λ_{ex} = 400 nm.

Having understood the photon cascade emission, one can easily understand the luminescence color change induced by varying λ_{ex} and P_{ex}. For $\lambda_{ex} < 392$ nm, the levels ^6G_J are not populated effectively and the photon cascade emission is not initiated. In this case, the population of the levels $^5D_3$ and $^5D_4$ in Tb^{3+} through Rabi oscillation or phonon assistance is dominant, giving rise to the four emission bands and green luminescence. For $\lambda_{ex} > 392$ nm, the electrons begin to occupy the levels ^6G_J, initiating the photon cascade emission which competes with the conventional emission. When the emission process becomes dominated by the photon cascade emission,

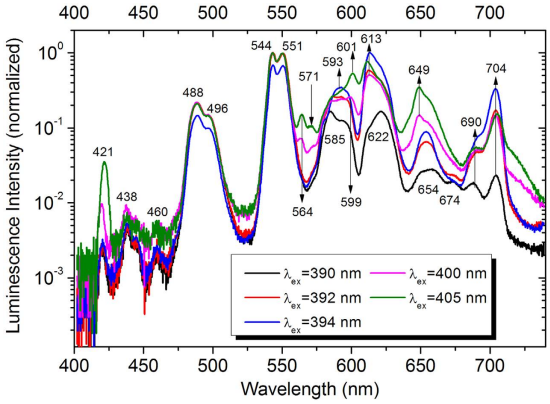

Figure 6. Comparison of the emission spectra of the glass plotted in a logarithmic coordinate under different λ_{ex} of 390, 392, 394, 400, and 405 nm. The new emission bands observed in the photon cascade emission are indicated by arrows.

the luminescence appears to be yellow or red. With increasing P_{ex}, the population of the level $^5D_3$ becomes significant because of two reasons. First, the population probability due to Rabi oscillation increases with increasing P_{ex}. Second, more electrons relax from the levels ^6G_J to the level $^5D_3$ after emitting two photons. Therefore, a rapid increase in the intensities of the emission bands at 488 and 544 nm is observed, turning the luminescence into yellow and green at high P_{ex}. In our case, it was found that the efficiency of the two-photon-induced transitions and ET process from Gd^{3+} to Tb^{3+} depends strongly on the concentrations of Gd^{3+} and Tb^{3+} because it is proportional to the inverse sixth power of the distance between the two types of ions (details in the Supplementary Information, see Section 5). In this work, we have compared the tunable range of the luminescence color by varying λ_{ex} and P_{ex} for several glass samples with different concentrations of Gd^{3+} and found that the best performance was achieved in the glass with the largest concentration of Gd^{3+}.

Conclusion

In conclusion, we have observed the two-photon-induced photon cascade emission in a glass codoped with Gd^{3+} and Tb^{3+} by using fs laser pulses. By varying either λ_{ex} or P_{ex}, we have demonstrated the manipulation of the luminescence color through the competition between the photon cascade emission and conventional emission. Many new emission bands, which are not usually observed in the traditional luminescence of Tb^{3+}-doped or Gd^{3+}/Tb^{3+}-codoped materials have been clearly revealed in the emission spectrum when the photon cascade emission is dominant. More importantly, the dependence of the luminescence on both λ_{ex} and P_{ex} implies potential applications in laser-induced color display.

Methods

Materials Preparation. The silicate glass was prepared through melting the mixture of analytical reagents of SiO_2, $Al(OH)_3$, Li_2CO_3, Gd_2O_3, and Tb_4O_7 at 1600 °C for 30 minutes. The melt was then poured onto a preheated (200 °C) stainless steel plate and annealed at 500 °C for 2 hours. The synthetized glass was cut into $10 \times 10 \times 1\,mm^3$ sheets and polished for optical measurements.

Photonluminescence Measurements. In our experiments, the fs laser light with a repetition rate of 76 MHz and a pulse duration of ~130 fs delivered by a Ti: sapphire oscillator (Mira 900S, Coherent) was introduced into a harmonic generator (Harmonics 9300, Coherent) and the output light with a tunable wavelength from 375 to 405 nm was employed to excite the glass. The excitation intensity was characterized by the peak power density of the fs laser pulses. It was introduced into an inverted microscope (Observer A1, Zeiss) and focused on the glass by using a 60 × objective lens (NA = 0.85). The diameter of the excitation spot was estimated to be ~4.0 μm. The luminescence generated by the glass was collected by the same objective lens and delivered to a spectrometer (SR-500I-B1, Andor) equipped with a charge-coupled device (CCD) (DU970N, Andor) for analysis. The photos of the excitation spot were taken by using a camera from the eyepiece of the microscope.

References

1. Wegh, R. T., Donker, H., Oskam, K. D. & Meijerink, A. Visible quantum cutting in $LiGdF_4:Eu^{3+}$ through downconversion. *Science* **283,** 663–666 (1999).
2. Kubota, S. & Shimada, M. $Sr_3Al_{10}SiO_{20}:Eu^{2+}$ as a blue luminescent material for plasma displays. *Appl. Phys. Lett.* **81,** 2749–2751 (2002).
3. Pust, P. *et al.* Narrow-band red-emitting $Sr[LiAl_3N_4]:Eu^{2+}$ as a next-generation LED-phosphor material. *Nat. Mater.* **13,** 891–896 (2014).
4. Ghosh, P., Tang, S. & Mudring, A. V. Efficient quantum cutting in hexagonal $NaGdF_4:Eu^{3+}$ nanorods. *J. Mater. Chem.* **21,** 8640–8644 (2011).
5. Lorbeer, C. & Mudring, A. V. Quantum cutting in nanoparticles producing two green photons. *Chem. Commun.* **50,** 13282–13284 (2014).
6. Lorbeer, C., Cybinska, J. & Mudring, A. V. Facile preparation of quantum cutting $GdF_3:Eu^{3+}$ nanoparticles from ionic liquids. *Chem. Commun.* **46,** 571–573 (2010).

7. Lorbeer, C., Cybinska, J. & Mudring, A. V. Reaching quantum yields » 100% in nanomaterials. J. M*ater. Chem. C* **2,** 1862–1868 (2014).
8. Zhang, Q. Y. & Huang, X. Y. Recent progress in quantum cutting phosphors. *Prog. Mater. Sci*. **55,** 353–427 (2010).
9. Fan, B., Chlique, C., Merdrignac-Conanec, O., Zhang, X. & Fan, X. Near-infrared quantum cutting material Er^{3+}/Yb^{3+} doped La_2O_2S with an external quantum yield higher than 100%. *J. Phys. Chem. C* **116,** 11652–11657 (2012).
10. Timmerman, D., Izeddin, I., Stallinga, P., Yassievich, I. N. & Gregorkiewicz, T. Space-separated quantum cutting with silicon nanocrystals for photovoltaic applications. *Nat. Photonics* **2,** 105–109 (2008).
11. van der Ende, B. M., Aarts, L. & Meijerink, A. Near-infrared quantum cutting for photovoltaics. *Adv. Mater.* **21,** 3073–3077 (2009).
12. van der Ende, B. M., Aarts, L. & Meijerink, A. Lanthanide ions as spectral converters for solar cells. *Phys. Chem. Chem. Phys.* **11,** 11081–11095 (2009).
13. Meijer, J. M. *et al.* Downconversion for solar cells in YF_3:Nd^{3+}, Yb^{3+}. *Phys. Rev. B* **81,** 035107 (2010).
14. Xu. Y. *et al.* Efficient near-infrared down-conversion in Pr^{3+}-Yb^{3+} codoped glasses and glass ceramics containing LaF_3 nanocrystals. *J. Phys. Chem. C* **115,** 13056–13062 (2011).
15. Heer, S., Lehmann, O., Haase, M. & Güdel, H. U. Blue, green, and red upconversion emission from lanthanide-doped $LuPO_4$ and $YbPO_4$ nanocrystals in a transparent colloidal solution. *Angew. Chem. Int. Ed.* **42,** 3179–3182 (2003).
16. Vetrone, F., Mahalingam, V. & Capobianco, J. A. Near-infrared-to-blue upconversion in colloidal $BaYF_5$:Tm^{3+}, Yb^{3+} nanocrystals. *Chem. Mater*. **21,** 1847–1851 (2009).
17. Mauser, N. *et al.* Tip enhancement of upconversion photoluminescence from rare earth ion doped nanocrystals. *ACS Nano* **9,** 3617–3626 (2015).
18. Pichaandi, J., Boyer, J. C., Delaney, K. R. & van Veggel, F. C. J. M. Two-photon upconversion laser (scanning and wide-field) microscopy using Ln^{3+}-doped $NaYF_4$ upconverting nanocrystals: a critical evaluation of their performance and potential in bioimaging. *J. Phys. Chem. C* **115,** 19054–19064 (2011).
19. Chen, G., Ohulchanskyy, T. Y., Kumar, R., Ågren, H. & Prasad, P. N. Ultrasmall monodisperse $NaYF_4$:Yb^{3+}/Tm^{3+} nanocrystals with enhanced near-infrared to near-infrared upconversion photoluminescence. *ACS Nano* **4,** 3163–3168 (2010).
20. Hua, R. *et al.* Visible quantum cutting in GdF_3:Eu^{3+} nanocrystals via downconversion. *Nanotechnology* **17,** 1642–1645 (2006).
21. Höppe, H. A. Recent developments in the field of inorganic phosphors. *Angew. Chem. Int. Ed.* **48,** 3572–3582 (2009).
22. Chen, G., Ohulchanskyy, T. Y., Kachynski, A., Ågren, H. & Prasad, P. N. Intense visible and near-infrared upconversion photoluminescence in colloidal $LiYF_4$:Er^{3+} nanocrystals under excitation at 1490 nm. *ACS Nano* **5,** 4981–4986 (2011).
23. Downing, E., Hesselink, L., Ralston, J. & Macfarlane, R. A three-color, solid-sate, three-dimensional display. *Science* **273,** 1185–1189 (1996).
24. Blasse, G. & Grabmaier, B. C. *Luminescent Materials*. (Springer-Verlag, Berlin, 1994).
25. Gai, S., Li, C., Yang, P. & Lin, J. Recent progress in rare earth micro/nanocrystals: soft chemical synthesis, luminescent properties, and biomedical applications. *Chem. Rev.* **114,** 2343–2389 (2014).
26. Zhou, J., Liu, Q., Feng, W., Sun, Y. & Li, F. Upconversion luminescent materials: advances and applications. *Chem. Rev*. **115,** 395–465 (2015).
27. Liu, Y., Tu, D., Zhu, H. & Chen, X. Lanthanide-doped luminescent nanoprobes: controlled synthesis, optical spectroscopy, and bioapplications. *Chem. Soc. Rev*. **42,** 6924–6958 (2013).
28. Nyk, M., Kumar, R., Ohulchanskyy, T. Y., Bergey, E. J. & Prasad. P. N. High contrast *in vitro* and *in vivo* photoluminescence bioimaging using near infrared to near infrared up-conversion in Tm^{3+} and Yb^{3+} doped fluoride nanophosphors. *Nano Lett.* **8,** 3834–3838 (2008).
29. Sotiriou, G. A., Franco, D., Poulikakos, D. & Ferrari, A. Optically stable biocompatible flame-made SiO_2-coated Y_2O_3:Tb^{3+} nanophosphors for cell imaging. *ACS Nano* **6,** 3888–3897 (2012).
30. Chen, G. *et al.* (α-$NaYbF_4$:Tm^{3+})/CaF_2 core/shell nanoparticles with efficient near-infrared to near-infrared upconversion for high-contrast deep tissue bioimaging. *ACS Nano* **6,** 8280–8287 (2012).
31. Bouzigues, C., Gacoin, T. & Alexandrou, A. Biological applications of rare-earth based nanoparticles. *ACS Nano* **5,** 8488–8505 (2011).
32. Heer, S., Kömpe, k., Güdel, H. U. & Haase, M. Highly efficient multicolour upconversion emission in transparent colloids of lanthanide-doped $NaYF_4$ nanocrystals. *Adv. Mater.* **16,** 2102–2105 (2004).
33. Bünzli, J. C. G. Lanthanide luminescence for biomedical analyses and imaging. *Chem. Rev*. **110,** 2729–2755 (2010).
34. Sudheendra, L. *et al.* $NaGdF_4$:Eu^{3+} nanoparticles for enhanced X-ray excited optical imaging. *Chem. Mater*. **26,** 1881–1888 (2014).
35. Damasco, J. A. *et al.* Size-tunable and monodisperse Tm^{3+}/Gd^{3+}-doped hexagonal $NaYbF_4$ nanoparticles with engineered efficient near infrared-to-near infrared upconversion for *in vivo* imaging. *ACS Appl. Mater. Interfaces* **6,** 13884–13893 (2014).
36. Ronda, C. R. Phosphors for lamps and displays: an applicational view. *J. Alloy. Comp*. **225,** 534–538 (1995).
37. Zhang, S., Zhu, B., Zhou, S., Xu, S. & Qiu, J. Multi-photon absorption upconversion luminescence of a Tb^{3+}-doped glass excited by an infrared femtosecond laser. *Opt. Express* **15,** 6883–6888 (2007).
38. Zanella, G. *et al.* A new cerium scintillating glass for X-ray detection. *Nucl. Instr. Meth. A* **345,** 198–201 (1994).
39. Eliseeva, S. V. *et al.* Multiphoton-excited luminescent lanthanide bioprobes: two- and three-photon cross sections of dipicolinate derivatives and binuclear helicates. *J. Phys. Chem. B* **114,** 2932–2937 (2010).
40. Zhou, S. S. *et al.* Synthesis, Optical properties and biological imaging of the rare earth complexes with curcumin and pyridine. *J. Mater. Chem*. **22,** 22774–22780 (2012).
41. Bettinelli, M., Carlos, L. & Liu, X. A new class of nanomaterials that convert near-IR radiation into tunable visible light has important implications for many fields of science and technology. *Phys. Today* **68(9),** 38–44 (2015).
42. Deng, R. *et al.* Temporal full-colour tuning through non-steady-state upconversion. *Nat. Nanotechnol*. **10,** 237–242 (2015).
43. Zhang, Y. *et al.* Multicolor barcoding in a single upconversion crystal. *J. Am. Chem. Soc.* **136,** 4893–4896 (2014).
44. Meruga, J. M., Baride, A., Cross, W., Kellara, J. J. & May, P. S. Red-green-blue printing using luminescence-upconversion inks. *J. Mater. Chem. C* **2,** 2221–2227 (2014).
45. Nikl, M. Scintillation detectors for X-rays. *Meas. Sci. Technol.* **17,** R37–R54 (2006).
46. Huang, S. & Gu, M. Enhanced luminescent properties of Tb^{3+} ions in transparent glass ceramics containing $BaGdF_5$ nanocrystals. *J. Non-Cryst. Solids* **358,** 77–80 (2012).
47. Reisfeld, R., Greenberg, E., Velapoldi, R. & Barnett, B. Luminescence quantum efficiency of Gd and Tb in borate glasses and the mechanism of energy transfer between them. *J. Chem. Phys.* **56,** 1698–1705 (1972).
48. Raju, G. S. R. *et al.* Gd^{3+} sensitization effect on the luminescence properties of Tb^{3+} activated calcium gadolinium oxyapatite nanophosphors. *J. Electrochem. Soc.* **158,** J20–J26 (2011).
49. Bril, A. & Wanmaker, W. L. Energy transfer in $CaNaBO_3$ activated with Tb and Gd. *J. Chem. Phys.* **43,** 2559–2560 (1965).
50. Han, B., Liang, H., Huang, Y., Tao, Y. & Su, Q. Vacuum ultraviolet-visible spectroscopic properties of Tb^{3+} in Li(Y, Gd)$(PO_3)_4$: tunable emission, quantum cutting, and energy transfer. *J. Phys. Chem. C* **114,** 6770–6777 (2010).
51. Zhang, C. F. *et al.* Femtosecond pulse excited two-photon photoluminescence and second harmonic generation in ZnO nanowires. *Appl. Phys. Lett.* **89,** 042117 (2006).
52. Li, G., Wang, W., Yang, W. & Wang, H. Epitaxial growth of group III-nitride films by pulsed laser deposition and their use in the development of LED devices. *Surf. Sci. Rep.* **70,** 380–423 (2015).

53. Yang, Z., Lin, J. H., Su, M. Z., Tao, Y. & Wang, W. Photon cascade luminescence of Gd^{3+} in $GdBaB_9O_{16}$. *J. Alloy. Comp.* **308,** 94–97 (2000).
54. Wegh, R. T., Donker, H., Meijerink, A., Lamminmäki, R. J. & Hölsä, J. Vacuum-ultraviolet spectroscopy and quantum cutting for Gd^{3+} in $LiYF_4$. *Phys. Rev. B* **56,** 13841–13848 (1997).

Acknowledgements

The authors acknowledge the financial support from the National Natural Science Foundation of China (Grant Nos. 51171066, 11374109, and 11204092) and the Scientific Research Foundation of the Graduate School of South China Normal University (Grant No. 2015lkxm01).

Author Contributions

S. Lan and M.-H. Yuan conceived the idea. S.-L.Tie and Z.-M. Yang fabricated the glass samples. M.-H. Yuan, H.-H. Fan, and H. Li carried out the optical experiments. S. Lan, M.-H. Yuan, S.-L. Tie, and Z.-M. Yang analyzed the data. M.-H. Yuan and S. Lan wrote the manuscript. S. Lan and S.-L. Tie supervised the project. All the authors read and commented on the manuscript.

Additional Information

Supplementary information accompanies this paper at http://www.nature.com/srep

Competing financial interests: The authors declare no competing financial interests.

How to cite this article: Yuan, M.-H. *et al.* Controlling the Two-Photon-Induced Photon Cascade Emission in a Gd^{3+}/Tb^{3+}-Codoped Glass for Multicolor Display. *Sci. Rep.* **6**, 21091; doi: 10.1038/srep21091 (2016).